Published in final edited form as:
Biochim Biophys Acta. 2015 January ; 1847(1): 109–118. doi:10.1016/j.bbabio.2014.06.008.

The pathway of O_2 to the active site in heme–copper oxidases★

Ólöf Einarsdóttir[a,*], **William McDonald**[a], **Chie Funatogawa**[a], **Istvan Szundi**[a], **William H. Woodruff**[c], and **R. Brian Dyer**[b]

[a]Department of Chemistry and Biochemistry, University of California, Santa Cruz, CA 95064, USA

[b]Department of Chemistry, Emory University, Atlanta, GA 30322, USA

[c]Santa Fe Institute, 1399 Hyde Park Road, Santa Fe NM 87501

Abstract

The route of O_2 to and from the high-spin heme in heme–copper oxidases has generally been believed to emulate that of carbon monoxide (CO). Time-resolved and stationary infrared experiments in our laboratories of the fully reduced CO-bound enzymes, as well as transient optical absorption saturation kinetics studies as a function of CO pressure, have provided strong support for CO binding to $\mathrm{Cu_B^+}$ on the pathway to and from the high-spin heme. The presence of CO on $\mathrm{Cu_B^+}$ suggests that O_2 binding may be compromised in CO flow-flash experiments. Time-resolved optical absorption studies show that the rate of O_2 and NO binding in the bovine enzyme (1×10^8 M^{-1} s^{-1}) is unaffected by the presence of CO, which is consistent with the rapid dissociation ($t_{1/2}$ = 1.5 μs) of CO from $\mathrm{Cu_B^+}$. In contrast, in *Thermus thermophilus* (*Tt*) cytochrome *ba*$_3$ the O_2 and NO binding to heme *a*$_3$ slows by an order of magnitude in the presence of CO (from 1×10^9 to 1×10^8 M^{-1} s^{-1}), but is still considerably faster (~10 μs at 1 atm O_2) than the CO off-rate from Cu_B in the absence of O_2 (milliseconds). These results show that traditional CO flow-flash experiments do not give accurate results for the physiological binding of O_2 and NO in *Tt ba*$_3$, namely, in the absence of CO. They also raise the question whether in CO flow-flash experiments on *Tt ba*$_3$ the presence of CO on $\mathrm{Cu_B^+}$ impedes the binding of O_2 to $\mathrm{Cu_B^+}$ or, if O_2 does not bind to $\mathrm{Cu_B^+}$ prior to heme *a*$_3$, whether the $\mathrm{Cu_B^+}$–CO complex sterically restricts access of O_2 to the heme. Both possibilities are discussed, and we argue that O_2 binds directly to heme *a*$_3$ in *Tt ba*$_3$, causing CO to dissociate from $\mathrm{Cu_B^+}$ in a concerted manner through steric and/or electronic effects. This would allow $\mathrm{Cu_B^+}$ to function as an electron donor during the fast (5 μs) breaking of the O–O bond. These results suggest that the binding of CO to $\mathrm{Cu_B^+}$ on the path to and from heme *a*$_3$ may not be applicable to O_2 and NO in all heme-copper oxidases. This article is part of a Special Issue entitled: Vibrational Spectroscopies in Molecular Bioenergetics.

★This article is part of a Special Issue entitled: Vibrational Spectroscopies in Molecular Bioenergetics.

*Corresponding author at: Physical Sciences Building, 1156 High Street, Santa Cruz, CA, 95064, USA. Tel.: +1 831 459 3155; fax: +1 831 459 2935. olof@ucsc.edu (Ó. Einarsdóttir).

Keywords

Time-resolved infrared spectroscopy; Time-resolved infrared linear dichroism; *Thermus thermophilus ba*$_3$; Photolabile O_2 and NO complex; CO photodissociation and recombination; dynamics

1. Introduction

Heme–copper oxidases, which include the cytochrome and ubiquinol oxidases, play a crucial role in energy production by aerobic organisms [1–3]. Their primary function is to catalyze the reduction of dioxygen to water using electrons from respiratory electron transport. The energy made available by the reaction generates a transmembrane electrochemical proton gradient that drives ATP synthesis [4]. These enzymes are responsible for over 90% of biological dioxygen reduction and for nearly half of the redox energy of cellular respiration [5,6]. Significantly, cytochrome *c* oxidase is inhibited by nitric oxide (NO) [7], a signaling molecule involved in diverse biochemical and physiological processes [8]. This inhibition of cytochrome oxidase may play an important role in regulating cellular respiration [7,9]. Several bacterial heme–copper oxidases are also able to catalyze the reduction of nitric oxide (NO) to nitrous oxide (N_2O) [10–13]; however, there are confiicting reports whether the bovine cytochrome oxidase has NO reductase activity [14,15].

The heme–copper oxidases are subdivided into three families, denoted A, B, and C [16,17], and all three families contain a high-spin heme (a_3, o_3 or b_3) which together with a copper center, Cu_B, forms the binuclear heme–copper site of O_2 binding and reduction. While sequence homology of the catalytic subunit containing the binuclear center is high between the bovine enzyme and the bacterial *Rhodobacter sphaeroides* (*Rs*) and *Paracoccus denitrificans (Pd) aa*$_3$ oxidases (54 and 55%, respectively), it is much lower in *Thermus thermophilus (Tt) ba*$_3$ and *Pseudomonas stutzeri cbb*$_3$ oxidases (23 and 15%, respectively). Despite this diversity, Cu_B in its oxidized form in all three oxidase families is trigonally ligated to the imidazole side chains of three conserved histidines, and the high-spin iron is ligated to an invariant histidine on the "proximal" side (opposite to the O_2 binding site) of the heme; in the *cbb*$_3$ oxidases, the proximal histidine is hydrogen bonded to the carboxylate of a glutamate residue [18]. All heme–copper oxidases also contain a post-translational modification, a cross-link between C6 of a tyrosine residue (Tyr 244 in the bovine enzyme) and the ε-nitrogen of one of the histidine ligands to Cu_B [19–21]. In the *cbb*$_3$ oxidases, the tyrosine originates from a different helix than in the A-and B-type oxidases [18].

Knowledge of the structural and dynamic features of the binuclear active site and the intraprotein channel(s) for ligation and proton transfer is critical for understanding the mechanisms of O_2 reduction, inhibition by NO, and NO reduction. The first step in O_2 reduction and NO inhibition and reduction relies on access of O_2 and NO, respectively, to the active site and how the protein environment modulates this access. Based on crystal structures, ligand pathways have been postulated for many heme–copper oxidases [18,20,22–25]. While there are significant sequence and structural similarities among these ligand pathways, there are variations in the global structure of the catalytic subunit, which may reflect the different functional environments of these enzymes. For instance, recent crystallographic studies of xenon (Xe) binding in *Tt* ba_3 [26] indicated that a constriction point in the oxygen channel of the aa_3 oxidases [24,27,28] is not present in *Tt* ba_3. This observation suggests easier access of ligands to the binuclear site in ba_3, which may be related to the different physiological requirements of the aa_3 and ba_3 oxidases [29].

Migration of O_2 through a ligand channel to the active site is followed by O_2 binding to the binuclear center. The role of Cu_B in transporting ligands such as O_2 and NO to and from the high-spin heme is of particular interest. Carbon monoxide (CO), a competitive inhibitor of O_2 reduction in cytochrome oxidase, has frequently been used as a model for O_2 binding [30–34], and the reactions following photodissociation of CO have been thought to exemplify the pathways of O_2 to and from the active site. This knowledge, however, is only relevant to the physiological O_2 reduction as long as the coordination chemistry of CO mimics that of O_2. The photodissociation of CO from the high-spin heme in the presence of O_2 has also been used extensively to initiate the O_2 reduction reaction [2,3,35–39]. However, the fate of the photodissociated CO may compromise the O_2 (or NO) binding and electron transfer dynamics [40]. This issue can only be addressed by exploring the photodissociation and recombination dynamics of the CO ligand, and by comparing the binding of O_2 and NO in the heme–copper oxidases in the presence of CO to the binding of these ligands under more realistic physiological conditions, namely, in the absence of CO.

In this review, we summarize vibrational and UV–vis spectroscopic studies of 1) the flash-induced photodissociation and rebinding of CO in the heme–copper oxidases, and 2) the reaction of O_2 with these enzymes in the presence and absence of CO. These results provide insight into the ligand binding dynamics of the heme-copper oxidases and how the protein environment modulates the ligand pathways and metal centers for different physiological environments.

2. CO photolysis and recombination dynamics

2.1. Fourier transform infrared (FTIR) experiments: CO binding to Cu_B^+

Characterization of the O_2 binding site is critical for understanding the mechanism of O_2 reduction to water and for elucidation of the protein structures that facilitate this reaction. Infrared spectroscopy provides a direct approach for studying the binding of ligands to heme proteins, including the heme–copper oxidases [30–34,41]. Carbon monoxide (CO) is commonly used as an infrared probe for O_2 binding because it generally binds to the same sites as O_2 and because of its strong infrared absorption and non-reducible nature. The frequencies and bandwidths of the CO infrared stretching bands can give valuable information not only about the identity of the metal center to which CO binds but also about the environment surrounding the CO ligand [31,34,41]. For example, CO binding to the high-spin heme in the bovine enzyme gives rise to a major peak at 1963 cm^{-1} (the Fe-bound C–O stretching frequency) in the infrared spectrum [31,34]. Infrared spectroscopy has also allowed us to follow the binding of CO to Cu_B^+, a metal center that is inaccessible to other spectroscopic techniques. Pioneering FTIR studies by Alben and coworkers showed that the photodissociated CO binds to Cu_B^+ in mitochondrial preparations under cryogenic conditions based on the infrared frequency at 2062 cm^{-1} [30,42].

Our laboratories have carried out extensive infrared studies of the photodissociation and recombination of the fully reduced CO-bound heme–copper oxidases [31,32,33,43–48]. FTIR difference spectra (dark minus light) were recorded over a wide temperature range (21–298 K) for the bovine enzyme, and *Tt* caa_3 and ba_3 [33]. Fig. 1 shows the spectra recorded between ~22 and 300 K for the bovine enzyme (left panels) and *Tt* ba_3 (right panels). In addition to the major heme a_3-CO band at 1963 cm^{-1}, the bovine enzyme has two minor bands at 1949 and 1944 cm^{-1}. At 21 K, *Tt* caa_3 shows two positive peaks at 1953 and 1947 cm^{-1} representing the heme a_3-CO [33], while CO binding to heme a_3 in *Tt* ba_3 gives rise to two major positive bands at 1974 and 1983 cm^{-1} (Fig. 1, right panels). The FTIR difference spectra show negative peaks at 2066, 2054 and 2039 cm^{-1} for the bovine enzyme, at 2060 and 2036 cm^{-1} for *Tt* caa_3 [33] and at 2054 cm^{-1} for *Tt* ba_3, which are attributed to CO binding to Cu_B^+.

The Cu_B^+-CO complex in the bovine and *Tt* caa_3 enzymes is kinetically stable below 140 K and 170 K, respectively, but dissociates at higher temperature. However, for *Tt* ba_3 we were able to observe binding of CO to Cu_B^+ upon continuous photolysis at room temperature in the FTIR dark-minus-light difference spectrum (Fig. 1, right panel, top spectrum). The differences in the CO stretching frequency for the Fe–CO (and Cu_B^+-CO) infrared absorption among these three oxidases indicate significant variations in the details of the CO binding and the stability of the Cu_B^+-CO intermediate. Nonetheless, the bandwidths of the IR peaks remain narrow over a large temperature range for all the oxidases, indicating a very homogeneous environment around the CO ligand. A recent combined crystallographic and infrared spectral study supports CO binding to Cu_B^+ in *Tt* ba_3 following photolysis of CO from heme a_3 [49].

We were also able to follow CO transfer from Cu_B^+ to Fe_{a3}^{2+} between 158 and 179 K in the bovine enzyme, 175–195 K in *Tt* caa_3 and 205–230 K in *Tt* ba_3 [33]. Taking into account the relative absorptivities of heme and copper CO-complexes, the relative integrated areas of the Fe–CO and Cu_B^+-CO infrared peaks represent quantitative transfer of CO from the heme to Cu_B following CO photodissociation, supporting a closed pocket isolated from the surrounding medium [32]. The activation parameters derived from an Eyring plot of the CO recombination in the three enzymes (Fig. 2) are listed in Table 1.

The multiple infrared heme–CO stretching bands represent discrete CO conformers of different structures that interconvert rapidly (on the FTIR time scale, i.e. minutes) [31,33]. For *Tt* ba_3, the Fe–CO conformers interconvert down to ~150 K, and they are energetically close as reflected by their relative populations between 180 K and room temperature. The thermodynamic parameters, ΔH^0 = 0.84 +/− 0.17 kcal/mol and ΔS^0 of 3.5 +/− 0.9 cal/mol-K, were obtained for the interconversion of the 1983 and 1974 cm^{-1} conformers based on the relative areas of the two conformers as a function of temperature [33]. These conformers were also observed in the CO-FTIR spectra of intact plasma membranes.

2.2. Resonance Raman experiments: multiple Fe–Im(N) conformers in Tt ba_3

We explored the different heme–copper oxidases by resonance Raman spectroscopy [48,50,51]. The resonance Raman spectra of the unliganded reduced *Tt* ba_3 in the low-frequency region, which contains the out-of-plane iron-imidazole nitrogen, Fe–N(Im), stretching vibration, show two bands around 192 and 208 cm^{-1} (Fig. 3). The use of isotopically enriched ^{57}Fe (95%) confirmed the assignments of these bands as the Fe–N(Im) stretching frequencies [51]. In contrast, the bovine enzyme shows a single Fe–N(Im) frequency at 214 cm^{-1}. The relative intensities of the two conformers in ba_3 are temperature dependent over a large range and track those of the Fe-CO peaks in the infrared spectra. This is reflected in almost identical thermodynamic parameters based on the Fe–CO (see above) and Fe–Im(N) conformer (ΔH^0 = 0.75 +/−1.2 kcal/mol and ΔS^0 of 2.1 +/− 1.2 cal/mol-K) thermodynamics plot (Fig. 4). This suggests that the Fe–CO infrared conformers and the Fe–N(Im) conformers arise from the same conformational changes, although the small thermodynamics values do not indicate major global structural changes. The different conformers may represent rotamers of the imidazole plane about the Fe–N axis, giving rise to different steric interactions between the imidazole and the heme of possible relevance to the coordination at the heme.

2.3. Dynamic time-resolved infrared (TRIR) experiments: Transient binding of CO to $\mathrm{Cu_B^+}$ at ambient temperature

While the low-temperature FTIR measurements provided important information about CO binding to $\mathrm{Cu_B^+}$ in the various heme–copper oxidases, it was imperative to demonstrate whether the photodissociated CO could also bind to $\mathrm{Cu_B^+}$ at room temperature, particularly with respect to CO flow-flash experiments that rely on the photolability of the CO complex to initiate the reaction with O_2. Time-resolved infrared (TRIR) spectroscopy of the photodissociated CO-bound bovine enzyme in our laboratories provided the first evidence for CO binding to $\mathrm{Cu_B^+}$ at room temperature following photodissociation of CO from heme a_3 [43]. Fig. 5 (top) displays the infrared transient at 2061 cm^{-1} due to the $\mathrm{Cu_B^+-CO}$ complex, and a single exponential fit shows that the $\mathrm{Cu_B^+-CO}$ transient decays with a half-life of 1.5 μs (Fig. 5, bottom). The time resolution of these early experiments was 200 ns but later experiments showed that CO binds to $\mathrm{Cu_B^+}$ within 3 ps [45]. More recent studies by others have shown photoinitiated CO ligand transfer to Cu_B of 60 fs [52]. The subsequent recombination of CO with Fe_{a3} occurs with an observed rate constant of ~90 s^{-1} at 1 atm of CO [32].

The photodissociated CO also binds to $\mathrm{Cu_B^+}$ in *Tt* caa_3 and ba_3 at room temperature following photodissociation of CO from heme a_3 as reflected by the infrared transients at 2036 cm^{-1} and 2054 cm^{-1}, respectively. In *Tt* caa_3, CO equilibrates with the surroundings on a microsecond time scale, 2×10^4 s^{-1}, and rebinds to heme a_3 with an apparent rate constant of 40 s^{-1} [47]. The room temperature infrared transients for *Tt* ba_3-CO before photolysis (1974 cm^{-1}; heme a_3-CO bound) and after photolysis (2053 $cm^{-1;}$ $\mathrm{Cu_B^+-CO}$) are shown in Fig. 6. The $\mathrm{Cu_B^+-CO}$ transient is much more stable in *Tt* ba_3 than in the bovine enzyme, and based on a single exponential fit decays with an apparent lifetime of ~46 ms, which is the same within experimental error as the value of 50 ms obtained for CO rebinding to heme a_3 (Fig. 6). These values are similar to those obtained previously (~30 s^{-1}) by time-resolved step-scan FTIR difference spectroscopy [53]. However, our UV–vis time-resolved optical absorption measurements show that the photodissociated CO rebinds to heme a_3 in ba_3 with an apparent lifetime of 260 ms, which is significantly slower than observed in our TRIR experiment and previous time-resolved step-scan FTIR measurements [53]. The cause of the discrepancy between the two approaches is unknown and is currently under investigation. Regardless, the slow CO dissociation from $\mathrm{Cu_B^+}$ in *Tt* ba_3 raises the question whether the photodissociated CO interferes with the reaction of *Tt* ba_3 with O_2. TRIR spectroscopy has also demonstrated the binding of the photodissociated CO to $\mathrm{Cu_B^+}$ in other heme–copper oxidases. For example, in *Escherichia coli* bo_3, CO dissociation from $\mathrm{Cu_B^+}$ was reported with a rate constant of ~500 s^{-1} [47], although later studies reported a multiphasic dissociation of CO from $\mathrm{Cu_B^+}$ on both microsecond and millisecond time scales [54]. The CO recombines with heme o_3 with an apparent rate constant of 40 s^{-1} (25 ms) based on UV–vis time-resolved optical absorption measurements in our laboratory.

2.4. Time-resolved infrared linear dichroism: the orientation of CO in heme a_3–CO and Cu_B–CO complexes of bovine aa_3

TRIR linear dichroism (TRIRLID) measurements allowed us to determine the orientation of the C–O bond axis with respect to the heme normal in the $\mathrm{Fe_{a3}^{2+}-CO}$ complex of the bovine enzyme as well as the $\mathrm{Cu_B^+-CO}$ photoproduct [44]. The TRIRLID is based on the differential absorption (photoselection) of parallel versus perpendicular polarized infrared light with respect to that of the photodissociation pulse and is measured as a function of the transmittance of the infrared probe beam. The results of such an experiment for both the Fe_{a3}–CO complex and the Cu_B–CO photoproduct of the bovine enzyme are shown in Fig. 7. TRIRLID experiments gave an angle between the heme normal and the C–O bond vector of 21° (+/−2°) for the $\mathrm{Fe_{a3}^{2+}-CO}$ in the bovine enzyme, which was supported by subsequent picosecond TRIR measurements [46]. For the $\mathrm{Fe_{a3}^{2+}-CO}$, a discrete angle (α) rather than a distribution of angles was assumed because the IR peak is very narrow, indicating the absence of inhomogeneous broadening [46]. The angle of 21° is in good agreement with an analogous angle of 16.6° derived based on the heme–CO bound crystal structure [55].

The TRIR linear dichroism technique also allowed us to determine the orientation of the C–O bond axis with respect to the heme normal in the $\mathrm{Cu_B^+-CO}$ transient photoproduct in the bovine enzyme. The TRIRLID signal for the transient photoproduct was practically the same for the parallel and perpendicular polarization of the infrared probe beam with respect to the photodissociation pulse (Fig. 7A, lower traces). The near absence of linear dichroism was interpreted in terms of angle, α, of 51 +/−3° between the heme normal and the C–O bond vector of the $\mathrm{Cu_B^+-CO}$ complex. Subsequent picosecond infrared measurements gave α of 55 +/− 3° [46]. It should be noted that the α values for the heme iron and Cu_B are cone half-angles because the TRIRLID does not provide angular orientation of the Fe_{a3}C–O and Cu_B–

CO vectors. Recent x-ray structure of the CO-bound bovine enzyme at 100 K indicates that CO is bound to Cu_B in a side-on fashion, with metal-to-carbon and metal-to-oxygen atom distances of 2.4 and 2.7 Å, respectively, indicating a weak Cu_B–CO bond [55]. Based on the crystal structure of the proposed Cu_B^+-CO complex (the crystal structure of the CO derivative determined at 100 K), the angle between the heme normal and the C–O bond vector for the Cu_B^+-CO complex is 65.5°, somewhat higher than observed in solution in the TRIRLID measurements. Based on a recent x-ray crystal structure of the CO-bound *Tt* ba_3 and the photodissociated product [49], the angle between the heme normal and the C–O bond vector is 66° for $Fe_{a3}^{2+}-CO$ and 64° for Cu_B^+-CO. Although the C–O bond vector for the Cu_B^+-CO complex makes a similar angle with respect to the heme normal in both the *Tt* ba_3 (64°) and bovine enzymes (65.5°), the CO is oriented within the binuclear center quite differently in these two enzymes as illustrated in Fig. 8. In the *Tt* ba_3 Cu_B^+-CO complex, the carbon atom is bonded to Cu_B^+ at a distance of 1.9 Å (top panel), while the oxygen atom is bonded to Fe_{a3} at a distance of 2.3 Å [49]. In addition, in the *Tt* ba_3 Cu_B^+-CO photoproduct, the ligand is directly above the Fe_{a3} atom along the heme normal vector. By contrast, the CO ligand is bound quite weakly to Cu_B in the bovine Cu_B–CO photoproduct, and the CO ligand is not above the Fe_{a3} atom, but is displaced away from Cu_B and the K-proton channel and toward the ligand entrance channel (Fig. 8, lower panel).

2.5. Transient UV–vis spectroscopy: the photodissociation and recombination dynamics of CO-cytochrome oxidase

While infrared spectroscopy has structural specificity and allows us to follow species that are inaccessible by other spectroscopic approaches, such as Cu_B^+-CO in cytochrome oxidase, transient UV–visible kinetic studies of the CO photodissociation and rebinding in a variety of heme proteins have provided important information about the heme environment and the dynamics of CO in the active site cavity and its migration pathways through the proteins [56,57]. In bovine cytochrome oxidase, an increase in the intensity of the α-band (615 nm) on picosecond time scale was observed following the initial femtosecond events accompanying the photodissociation of CO from heme a_3 [32]. A subsequent decrease in the α-band was observed on ~1 μs times scale, simultaneously with the loss of CO from Cu_B^+. These picosecond and microsecond changes were associated with structural effects at heme a_3 following the formation and dissociation of the Cu_B^+-CO complex [32]. The observed pseudo-first-order rate of rebinding of the flash-dissociated CO to cytochrome a_3 of the bovine heart enzyme showed the onset of saturation at [CO] >1 mM (P_{CO} ~1–22 atm) when measured at room temperature on micro- and millisecond time scales. This was interpreted in terms of CO, and by extension other ligands such as O_2, first binding to a non-heme site, i.e. Cu_B^+, as it migrated to heme a_3. Saturation kinetics was also reported for the rebinding of the photodissociated CO to *E. coli* bo_3 ubiquinol oxidase as a function of CO concentration [58]. Interestingly, two mutant oxidases (His333Leu and His334Leu), in which the Cu_B site was significantly altered, or Cu_B was lacking, showed no evidence of CO binding saturation up to 21 mM CO. This was interpreted as Cu_B acting as a way-station for CO moving to the heme. In contrast, in *Tt* ba_3, the observed rate constant for CO rebinding to the heme a_3

appears to be independent of CO over a large concentration range, 25 μM–3 mM [47]. This indicates that the pre-equilibrium of CO with a non-heme site, i.e. Cu_B, in *ba*$_3$ is saturated at the lowest CO concentration used.

The TRIR and transient UV–visible results of the kinetics of CO rebinding following its photodissociation from the high-spin heme have been explained by the kinetics model shown in Scheme 1, which includes an obligatory binding of CO to $\mathrm{Cu_B^+}$ to and from the high-spin heme. In Scheme 1, k_1 represents CO binding to Cu_B from solution prior to the rate-limiting CO transfer to $\mathrm{Fe_{a3}^{2+}}$, represented by k_2. The thermal dissociation of CO from $\mathrm{Fe_{a3}^{2+}}$ is represented by k_{-2}. The equilibrium constants are represented by $K_1 = k_1/k_{-1}$ and $K_2 = k_2/k_{-2}$. Based on our CO recombination kinetics of the bovine enzyme as a function of CO concentration, we calculated a value for k_{-2} of 0.027 s^{-1}, which is in excellent agreement with the value of 0.023 s^{-1}, reported previously by Gibson and Greenwood [36]. In *Tt ba*$_3$, this rate is much faster or 0.8 s^{-1} [59].

3. O_2 and NO binding in heme–copper oxidases in the absence and presence of CO

If the binding of CO to Cu_B in the heme-copper oxidases precedes the binding of CO to the high-spin heme, does this binding affect the access of other ligands, such as O_2 and NO, to the active site in CO/NO and CO/O_2 flow-flash experiments? As shown above, the $\mathrm{Cu_B^+{-}CO}$ complex decays with a half-life of ~1.5 μs in the bovine enzyme [32,43] while in *Tt ba*$_3$ the $\mathrm{Cu_B^+{-}CO}$ complex decays on a millisecond time scale (Fig. 6 and [53]), much slower than that of O_2 binding to heme a_3^{2+} in the *aa*$_3$ oxidases (~10–20 μs at ~0.5–1 mM O_2). This long lifetime of the $\mathrm{Cu_B^+{-}CO}$ complex in *ba*$_3$ raises questions whether O_2 binding to heme a_3 may be impeded by the binding of the photodissociated CO to $\mathrm{Cu_B^+}$ in CO/O_2 flow-flash experiments on this enzyme, and secondly, whether the binding of O_2 and NO to $\mathrm{Cu_B^+}$ on route to heme a_3 is a general feature of the ligand binding dynamics of the heme–copper oxidases as observed for CO. Results from studies aimed at answering these questions are summarized below.

3.1. Does CO impede O_2 and NO access to the active site in heme-copper oxidases?

To investigate whether CO impedes access of O_2 and NO to the active site in the heme-copper oxidases, we monitored the reactions of O_2 and NO with bovine *aa*$_3$ and *Tt ba*$_3$ under more physiological conditions, namely, in the absence of CO using time-resolved optical absorption spectroscopy in combination with photolabile O_2 and NO carriers [40, 60]. This technique eliminates the possible interferences from the photodissociated CO in typical CO flow-flash experiments as well as circumvents the low NO quantum yield in NO flash-photolysis studies. The results from these studies were compared to those obtained in the presence of CO using a double-laser approach in which the O_2 and NO were generated by photolyzing the respective O_2 and NO photolabile carrier with a 355 nm laser pulse and the CO-bound enzyme was photolyzed simultaneously using a second 532 nm laser pulse [40,60]. Time-resolved optical absorption spectra were recorded and the data were analyzed with a combination of singular value decomposition (SVD), global exponential fitting and an algebraic kinetic approach and the spectra of the intermediates were determined. The data show that O_2 and NO bind to cytochrome a_3 in *Tt* ba_3 in the absence of CO with a second order rate constant of 1×10^9 M^{-1} s^{-1}, which is 10-times faster than observed in the bovine enzyme (1×10^8 M^{-1} s^{-1}) under the same conditions [40,60]. Moreover, the O_2 and NO binding in *Tt* ba_3 is 10-times slower in the presence of CO (1×10^8 M^{-1} s^{-1}) while the presence of CO does not affect the rate of O_2 and NO binding in the bovine enzyme (Fig. 9). These results show that the reactions of O_2 and NO with reduced *Tt* ba_3 are indeed compromised by the transient binding of the photodissociated CO to Cu_B^+ and that the CO flow-flash method does not give accurate results for "physiological" O_2 and NO binding in ba_3, i.e. that observed in the absence of CO.

The post-photolysis structure of the bovine enzyme shows that CO is quite weakly bound to Cu_B^+ [55], while CO is bound much more tightly to Cu_B in *Tt* ba_3 [49]. For example, the Cu_B–C distance is 2.4 Å and 1.9 Å in the bovine and ba_3 structures, respectively [49,55]. Likewise, the Fe–O distance is 3.8 Å (not bound) and 2.3 Å in the bovine and ba_3 post-photolysis structures, respectively. It is noteworthy that the CO in the post-photolysis bovine enzyme moves "out" of the binuclear center, i.e. away from the H_2O exit channel and back toward the ligand entrance channel. This suggests that in the post-photolysis fully reduced CO-bound bovine enzyme, CO is already "escaping" the binuclear center; this is in contrast to the ba_3 enzymes, in which the photodissociated CO rotates within the binuclear cavity, but remains bound to the metals. This may explain why CO impedes O_2 binding in ba_3 but not in the bovine enzyme.

3.2. Differences in ligand access to the active site in bovine aa_3 and Tt ba_3

The 10-fold faster rate of O_2 and NO binding in *Tt* ba_3 compared to bovine aa_3 in the absence of CO indicates inherent structural differences between ligand access in the two enzymes, which may reflect their different physiological requirements. In the aa_3 oxidases, a constriction point defined by conserved tryptophan and phenylalanine residues was identified [24,27,28], while in *Tt* ba_3 these sites are occupied by smaller residues, tyrosine (Y133) and threonine (T231), respectively [26]. Recent experiments in our laboratory have shown that O_2 and NO binding to heme a_3 in the absence of CO in the Y133W and Y133W/T231F mutants of *Tt* ba_3 is ~5 times slower than in the wild type enzyme [29]. This suggests that the significantly slower ligand binding in the bovine enzyme (1×10^8 M^{-1} s^{-1}) compared to that in *Tt* ba_3 (1×10^9 M^{-1} s^{-1}) in the absence of CO is in part due to the tryptophan constriction residue in the ligand channel of the bovine aa_3 (W126) impeding O_2 and NO access to the active site [29]. Interestingly, mutation of the T231 residue in *Tt* ba_3 to the corresponding phenylalanine in the aa_3 oxidases did not have any effect on the ligand binding rate [29]. Classical molecular dynamics simulations of Xe and O_2 diffusion to the active sites in ba_3 and bovine aa_3 showed that the native bovine F238 residue and the F231 side chain of the Y133W/T231F mutant, which in the crystal structures extend into the ligand channels, rotate out of the channels, resulting in no effect on ligand access in the T231F mutant and, by extension, in the bovine enzyme [29]. The rate of O_2 and NO binding in the Y133W and Y133W/T231F mutants of *Tt* ba_3 in the presence of CO was also 10-

times slower than in the corresponding mutants in the absence of CO and 50 times slower than in the wild-type enzyme in the absence of CO. This demonstrates that the photodissociated CO directly or indirectly slows down ligand binding in the mutants to the same extent as in the wild type *Tt* ba_3.

3.3. How does CO impede access of O_2 and NO to the active site in Tt ba_3?

In the mitochondrial enzyme, the $Cu_B^+ - CO$ photoproduct decays with a half-life of ~1.5 μs based on the TRIR transient at 2062 cm^{-1} [32,43], significantly faster than the ~10 μs binding of O_2 to heme a_3 (at 625 μM [O_2]) observed in either the absence or presence of CO. Thus the dissociation of CO from Cu_B does not limit O_2 or NO binding at the active site (Cu_B or heme a_3) in the bovine enzyme at this O_2 concentration.

In the absence of CO, the rate of O_2 and NO binding to heme a_3 in *Tt* ba_3 is close to the diffusion-controlled limit. Therefore, if O_2 and NO were to bind to Cu_B^+ prior to heme a_3 in *Tt* ba_3, this obligatory binding would not appear to limit access of the ligands to heme a_3. Even in the presence of CO, the O_2 and NO binding in *Tt* ba_3 is $1 \times 10^8 M^{-1} s^{-1}$ (~ 10 μs at 625 μM O_2), significantly faster than the millisecond CO dissociation from Cu_B observed in the absence of O_2.

If CO remains on Cu_B^+ in *Tt* ba_3 on millisecond time scale in the presence of O_2 and the active site is only able to accommodate one ligand at the active site, O_2 or NO would not be able to bind to the heme, which is clearly not the case. On the other hand, if the active site is able to accommodate two ligands, albeit transiently, and if the photodissociated CO stays bound to Cu_B^+ in *Tt* ba_3 for tens of milliseconds in the presence of O_2, then Cu_B would not be an obligatory way-station for O_2 (or NO) binding to heme a_3. In this case, O_2 (NO) would presumably bind to heme a_3 with CO remaining on Cu_B^+. However, a prolonged presence of CO on Cu_B would not allow Cu_B to act as an electron donor for the rapid O–O bond cleavage (4–5 μs) observed during O_2 reduction in ba_3 both in the absence [40,60] and presence of CO [61]. This leads us to the conclusion that the photodissociated CO in ba_3 does not remain on Cu_B for a prolonged period of time (hundred of microseconds) when O_2 is present but still long enough to decrease the O_2 binding rate to the high-spin heme by an order of magnitude. The binding of CO to Cu_B in *Tt* ba_3 could either impede the binding of O_2 to Cu_B^+ or if O_2 does not bind to Cu_B^+ prior to heme a_3, the $Cu_B^+ - CO$ complex could sterically restrict access of O_2 to the heme. The two scenarios will be discussed in more detail below.

3.4. Is Cu_B^+ an obligatory gate for O_2 binding to the high-spin heme in bovine aa_3 and Tt ba_3?

The binding of O_2 in the heme–copper oxidases has been proposed to follow Scheme 1, namely, that the obligatory path of O_2 to and from the high-spin heme involves the transient binding of O_2 to Cu_B^+, as observed for CO. In early flow-flash studies of the reaction of the reduced bovine enzyme with O_2, the fast phase was found to increase proportionally with O_2 concentration at low concentrations but saturate at higher concentration (~1 mM) [37,62].

Later studies used two lasers to study the kinetics of O_2 binding in the bovine enzyme as a function of O_2 concentration, in which the first pulse photolyzed the heme a_3–CO complex and the second pulse photolyzed the early transient species in the O_2 reaction, presumably the heme $a_3^{2+}-O_2$ complex [63]. The authors found that the fast component of the reaction displayed a rate limit at higher O_2 concentration (up to 700 μM). However, there was no evidence of rate limitation in the flow-flash experiment with NO, and the authors suggested that if the escape of CO from the active site in the bovine enzyme was the cause of the O_2 saturation kinetics, such a mechanism would not be in place for NO; these types of measurements have not been carried out on *Tt ba*$_3$. It should be noted that the limited O_2 concentration in these experiments of 1 mM or less makes it difficult to ascertain unequivocally saturation kinetics behavior at high O_2 concentrations as well as separate the redox processes following O_2 binding. Subsequent high O_2 pressure flow-flash studies of the reaction of dioxygen with the bovine enzyme (up to 16 mM O_2) reported that the rate of O_2 binding showed saturation kinetics at high O_2 con- centration with a limiting rate constant of 1×10^6 s^{-1} [64]. It was suggested that this rate (~1 μs) was set by the dissociation of CO from $\mathrm{Cu_B^+}$, which occurs at approximately the same rate. The authors concluded that either the $\mathrm{Cu_B^+}-\mathrm{O_2}$ complex forms prior to transfer of O_2 to the high-spin heme or that the $\mathrm{Cu_B^+}-\mathrm{CO}$ directly blocks access of the incoming O_2 to the heme. However, as discussed above, at ~625 μM O_2 concentration the lifetime of the $\mathrm{Cu_B^+}-\mathrm{CO}$ photoproduct of the bovine enzyme is too short (1.5 μs) to interfere with the ~10 μs O_2 binding. High O_2 pressure flow-flash measurements have not been carried out on the reaction of O_2 with *Tt ba*$_3$. In an FTIR study of the steady-state *Tt ba*$_3$ CO complex in the presence of limited amount of O_2 (70 μM), the C–O stretching frequency of the Cu_B–CO complex was found to shift from the usual 2053 cm^{-1} to 2045 cm^{-1} [65]. The latter peak belonged to CO as demonstrated by the appropriate shift in the ^{13}CO spectrum. These results were interpreted as being the result of structural changes at Cu_B caused by O_2 being close to but not bound to Cu_B.

3.5. Does the $\mathrm{Cu_B^+}-\mathrm{CO}$ complex directly block access of O_2 to heme a_3 in Tt ba_3?

Alternatively, O_2 may not bind to $\mathrm{Cu_B^+}$ in the heme–copper oxidases, in particular in *Tt ba*$_3$, prior to being transferred to the high-spin heme. In the case of *ba*$_3$, the direct binding of O_2 to heme a_3 may give rise to changes in the geometry around Cu_B from tetrahedrally-distorted square planar to more square planar, which in a concerted manner could give rise to the dissociation of CO from $\mathrm{Cu_B^+}$, thus allowing Cu_B to act as an electron donor to the bound dioxygen. This would require the active site in *Tt ba*$_3$ to be able to transiently accommodate two ligand molecules, CO on Cu_B and O_2 on heme a_3. The relatively short distance between heme and $\mathrm{Cu_B^+}$ in *Tt ba*$_3$ (4.4 Å) [66] compared to that in bovine *aa*$_3$ (5.1 Å) [67] would likely preclude the simultaneous binding of CO to $\mathrm{Cu_B^+}$ and either O_2 (or NO) to heme a_3^{2+} without some conformational changes [68]. Such structural changes as a result of ligand binding to heme a_3 are supported by time-resolved magnetic circular dichroism and circular dichroism measurements of the unligated *Tt ba*$_3$ formed after photodissociation of its CO complex [69]. These measurements showed spectral differences between the photolyzed enzyme and the steady-state unliganded enzyme, which were explained in terms of CO binding to heme a_3 inducing a global conformational change at the active site, which persisted on a time scale comparable to that of CO rebinding. Both the "dark" heme a_3–CO and "light" Cu_B^+-CO structures [49] show a structural distortion in heme a_3, with somewhat greater distortion (the porphyrin being not planar) in the dark structure. The Fe_{a3}–Cu_B distance increases from 4.7 Å in the "dark" structure to 5.1 Å in the "light" structure, which may be due to tighter binding of CO to Cu_B than to Fe_{a3}. It should also be noted that the crystal structure of *Tt ba*$_3$ shows that the high spin heme a_3 is tilted away from Cu_B, thus providing a larger surface area to the incoming ligand than in the *aa*$_3$ oxidases. This might allow a second ligand to be accommodated at the active site, an essential requirement of the NO reductase activity of this enzyme [12]. Based on theoretical studies, Blomberg and coworkers have proposed that two NO molecules bind at the active site of *Tt ba*$_3$, one to heme a_3 and one to Cu_B (through the two oxygen atoms) during the conversion of NO to N_2O [70]. Low-temperature FTIR photolysis experiments of the *ba*$_3$–NO complex led to the proposal of a Fe_{a3}–NO NO–Cu_B intermediate during the NO reductase reaction, suggesting that the *ba*$_3$ binuclear center is able to transiently bind two ligands [71]. Previous spectroscopic measurements also show that two CN^- molecules can be accommodated simultaneously at the active site of *Tt ba*$_3$, one bound to Fe_{a3}^{2+} and the other one to Cu_B^{2+} [72]. Several studies have reported that the A-type oxidases can simultaneously accommodate two ligands at the active site [14,15,73–76].

4. Conclusions

Several important conclusions can be drawn from the results described here. 1) Our infrared experiments, as well as UV–vis saturation CO rebinding studies as a function of CO pressure provide strong evidence that the obligatory path of CO to and from the high-spin heme in the heme–copper oxidases involves the transient binding of CO to Cu_B^+. 2) Our TRIRLID measurements allowed us to determine the orientation of the C–O bond axis with respect to the heme normal in both the heme a_3–CO complex and the Cu_B–CO product of the bovine enzyme, and the results are in good agreement with later crystallographic results. 3) Our time-resolved optical absorption measurements show superfast O_2 and NO binding to Fe_{a3} in *Tt ba*$_3$ in the absence of CO, $1 \times 10^9\ M^{-1}\ s^{-1}$, which approaches the diffusion-controlled limit and is 10-times faster than in the bovine enzyme under the same conditions. The slower O_2 and NO binding in the bovine enzyme compared to *ba*$_3$ is partially due to the tryptophan constriction point residue in the O_2 channel of the bovine enzyme impeding access of O_2 and NO to the active site. The more open channel in *Tt ba*$_3$, which allows easier access of O_2 to the heme, likely reflects the functional requirements of the thermophilic bacterium, which is found under microaerobic conditions and grows optimally at 70 °C (at which temperature O_2 solubility is half of that in water at 25 °C). 4) The rate of O_2 and NO binding is 10-times slower in the presence of CO while in the bovine enzyme the O_2 and NO binding rate is the same in the presence and absence of CO ($1 \times 10^8\ M^{-1}\ s^{-1}$). These results indicate that the CO flow-flash method does not accurately reflect the O_2 and NO binding in *Tt ba*$_3$ under physiological conditions, namely, in the absence of CO.

Despite considerable progress, there are still some outstanding issues regarding ligand binding in the heme–copper oxidases, most importantly whether the route of O_2 (NO) to and from the high-spin heme involves an obligatory binding to Cu_B, as has been proposed for CO, and whether this path is the same for all heme–copper oxidases. While the CO flow-flash UV–visible measurements carried out at high O_2 pressure on the bovine enzyme reported a nonlinear dependence of the observed rate of O_2 binding as a function of O_2 concentration [64], no saturation limit was observed in flow-flash experiments on the binding of NO to the bovine enzyme [63], a ligand that is expected to model O_2 binding. In the bovine enzyme, our TRIR experiments show that CO dissociates from Cu_B with a half-life of 1.5 μs, rapidly enough not to interfere with ~10 μs O_2 (NO) binding to heme a_3 at 1 mM O_2. Moreover, the rate of O_2 binding to heme a_3 is the same in the presence and absence of CO, indicating that the $\mathrm{Cu}_\mathrm{B}^+-\mathrm{CO}$ complex is not sterically restricting access of O_2 to the heme. Thus the evidence is inconclusive whether Cu_B^+ acts a way-station for O_2 (NO) in the bovine enzyme.

In *Tt ba*$_3$, our UV–visible results show that the binding of the photodissociated CO to Cu_B^+ slows the access of O_2 (NO) to heme a_3 by an order of magnitude compared to that observed in the absence of CO. The Cu_B in *ba*$_3$ has significantly higher affinity for CO compared to the bovine enzyme [47], and the crystal structure of the Cu_B–CO complex shows that the Cu_B–C bond is significantly shorter (1.88 Å) [49] and stronger than the corresponding bond in the bovine enzyme (2.43 Å) [55]. Thus it seems unlikely that O_2 would replace CO on Cu_B^+. If CO remains bound to Cu_B for longer than a few microseconds, Cu_B^+ would not be able to provide one of the electrons required for the rapid (5 μs) breaking of the O–O bond. This is clearly not the case. We propose that the direct binding of O_2 to heme a_3 in *Tt ba*$_3$ and the driving force for the breaking of the O–O bond cause CO to dissociate from Cu_B^+ in a concerted manner through steric and/or electronic effects, thereby allowing Cu_B^+ to act as an electron donor during the breaking of the O–O bond. For this to happen would require the transient presence of two ligands, one on heme a_3 and the other on Cu_B. This proposal is supported by the NO reductase activity of *Tt ba*$_3$, which would require two NO molecules to be transiently bound at the active site. FTIR studies aimed at resolving whether the active site in *Tt ba*$_3$ is indeed able to accommodate two ligands are in progress.

Acknowledgments

This work was supported by the National Science Foundation Grant CHE-1158548 (ÓE) and the National Institutes of Health Grants GM068036 (BD).

References

1. Brzezinski P, Larsson G. Redox-driven proton pumping by heme–copper oxidases. Biochim Biophys Acta. 2003; 1605:1–13. [PubMed: 12907296]
2. Einarsdóttir Ó. Fast reactions of cytochrome oxidase. Biochim Biophys Acta. 1995; 1229:129–147. [PubMed: 7727494]
3. Ferguson-Miller S, Babcock GT. Heme/copper terminal oxidases. Chem Rev. 1996; 96:2889–2907. [PubMed: 11848844]

4. Wikström MKF. Proton pump coupled to cytochrome *c* oxidase in mitochondria. Nature. 1977; 266:271–273. [PubMed: 15223]
5. Chan SI, Li PM. Cytochrome *c* oxidase: understanding nature's design of a proton pump. Biochemistry. 1990; 29:1–12. [PubMed: 2157476]
6. Wikström, M.; Krab, K.; Saraste, M. Cytochrome Oxidase—A Synthesis. Academic Press; New York: 1981.
7. Brown GC. Regulation of mitochondrial respiration by nitric oxide inhibition of cytochrome *c* oxidase. Biochim Biophys Acta. 2001; 1504:46–57. [PubMed: 11239484]
8. Ignarro, LJ. Nitric Oxide: Biology and Pathobiology. Academic Press; San Diego, CA: 2000.
9. Brunori M, Giuffrè A, Forte E, Mastronicola M, Barone BC, Sarti P. Control of cytochrome *c* oxidase activity by nitric oxide. Biochim Biophys Acta. 2004; 1655:365–371. [PubMed: 15100052]
10. Butler CS, Forte E, Scandurra FM, Arese M, Giuffrè A, Greenwood C, Sarti P. Cytochrome bo_3 from *Escherichia coli*: the binding and turnover of nitric oxide. Biochem Biophys Res Commun. 2002; 296:1272–1278. [PubMed: 12207912]
11. Forte E, Urbani A, Saraste M, Sarti P, Brunori M, Giuffrè A. The cytochrome cbb_3 from *Pseudomonas stutzeri* displays nitric oxide reductase activity. Eur J Biochem. 2001; 268:6486–6491. [PubMed: 11737203]
12. Giuffrè A, Stubauer G, Sarti P, Brunori M, Zumft WG, Buse G, Soulimane T. The heme–copper oxidases of *Thermus thermophilus* catalyze the reduction of nitric oxide: evolutionary implications. Proc Natl Acad Sci U S A. 1999; 96:14718–14723. [PubMed: 10611279]
13. Huang Y, Reimann J, Lepp H, Drici N, Ädelroth P. Vectorial proton transfer coupled to reduction of O_2 and NO by a heme–copper oxidase. Proc Natl Acad Sci U S A. 2008; 105:20257–20262. [PubMed: 19074284]
14. Stubauer G, Giuffrè A, Brunori M, Sarti P. Cytochrome *c* oxidase does not catalyze the anaerobic reduction of NO. Biochem Biophys Res Commun. 1998; 245:459–465. [PubMed: 9571175]
15. Zhao XJ, Sampath V, Caughey WS. Cytochrome *c* oxidase catalysis of the reduction of nitric oxide to nitrous oxide. Biochem Biophys Res Commun. 1995; 212:1054–1060. [PubMed: 7626092]
16. Hemp J, Gennis RB. Diversity of the heme–copper superfamily in *Archaea*: insights from genomics and structural modeling. Results Probl Cell Differ. 2008; 45:1–31. [PubMed: 18183358]
17. Pereira MM, Santana M, Teixeira M. A novel scenario for the evolution of haem–copper oxygen reductases. Biochim Biophys Acta. 2001; 1505:185–208. [PubMed: 11334784]
18. Buschmann S, Warkentin E, Xie H, Langer JD, Ermler U, Michel H. The structure of cbb_3 cytochrome oxidase provides insights into proton pumping. Science. 2010; 329:327–330. [PubMed: 20576851]
19. Ostermeier C, Harrenga A, Ermler U, Michel H. Structure at 2.7 Å resolution of the *Paracoccus denitrificans* two-subunit cytochrome *c* oxidase complexed with an antibody FV fragment. Proc Natl Acad Sci U S A. 1997; 94:10547–10553. [PubMed: 9380672]
20. Soulimane T, Buse G, Bourenkov GP, Bartunik HD, Huber R, Than ME. Structure and mechanism of the aberrant ba_3-cytochrome *c* oxidase from *Thermus thermophilus*. EMBO J. 2000; 19:1766–1776. [PubMed: 10775261]
21. Yoshikawa S, Shinzawa-Itoh K, Nakashima R, Yaono R, Yamashita E, Inoue N, Yao M, Fei MJ, Libeu CP, Mitzushima T, Yamaguchi H, Tomizaki T, Tsukihara T. Redox-coupled crystal structural changes in bovine heart cytochrome *c* oxidase. Science. 1998; 280:1723–1731. [PubMed: 9624044]
22. Abramson J, Riistama S, Larsson G, Jasaitis A, Svensson-Ek M, Laakkonen L, Puustinen A, Iwata S, Wikström M. The structure of the ubiquinol oxidase from *Escherichia coli* and its ubiquinone binding site. Nat Struct Biol. 2000; 7:910–917. [PubMed: 11017202]
23. Iwata S, Ostermeier C, Ludwig B, Michel H. Structure at 2.8 Å resolution of cytochrome *c* oxidase from *Paracoccus denitrificans*. Nature. 1995; 376:660–669. [PubMed: 7651515]
24. Svensson-Ek M, Abramson J, Larsson G, Törnroth S, Brzezinski P, Iwata S. The X-ray crystal structures of wild-type and EQ(I-286) mutant cytochrome *c* oxidases from *Rhodobacter sphaeroides*. J Mol Biol. 2002; 321:329–339. [PubMed: 12144789]

25. Tsukihara T, Aoyama H, Yamashita E, Tomizaki T, Yamaguchi H, Shinzawa-Itoh K, Nakashima R, Yaono R, Yoshikawa S. The whole structure of the 13-subunit oxidized cytochrome *c* oxidase at 2.8 Å. Science. 1996; 272:1136–1144. [PubMed: 8638158]

26. Luna VM, Chen Y, Fee JA, Stout CD. Crystallographic studies of Xe and Kr binding within the large internal cavity of cytochrome ba_3 from *Thermus thermophilus*: structural analysis and role of oxygen transport channels in the heme-Cu oxidases. Biochemistry. 2008; 47:4657–4665. [PubMed: 18376849]

27. Hofacker I, Schulten K. Oxygen and proton pathways in cytochrome *c* oxidase. Proteins Struct Funct Genet. 1998; 30:100–107. [PubMed: 9443344]

28. Salomonsson L, Lee A, Gennis RB, Brzezinski P. A single-amino-acid lid renders a gas-tight compartment within a membrane-bound transporter. Proc Natl Acad Sci U S A. 2004; 101:11617–11621. [PubMed: 15289603]

29. McDonald W, Funatogawa C, Li Y, Szundi I, Chen Y, Fee JA, Stout CD, Einarsdottir Ó. Ligand access to the active site in *Thermus thermophilus* ba_3 and bovine heart aa_3 cytochrome oxidases. Biochemistry. 2013; 52:640–652. [PubMed: 23282175]

30. Alben JO, Moh PP, Fiamingo FG, Altschuld RA. Cytochrome oxidase (a_3) heme and copper observed by low-temperature Fourier transform infrared spectroscopy of the CO complex. Proc Natl Acad Sci U S A. 1981; 78:234–237. [PubMed: 6264435]

31. Einarsdóttir Ó, Choc MG, Weldon S, Caughey WS. The site and mechanism of dioxygen reduction in bovine heart cytochrome *c* oxidase. J Biol Chem. 1988; 263:13641–13654. [PubMed: 2843526]

32. Einarsdóttir Ó, Dyer RB, Lemon DD, Killough PM, Hubig SM, Atherton SJ, López-Garriga JJ, Palmer G, Woodruff WH. hotodissociation and recombination of carbonmonoxy cytochrome oxidase: dynamics from picoseconds to kiloseconds. Biochemistry. 1993; 32:12013–12024. [PubMed: 8218278]

33. Einarsdóttir Ó, Killough PM, Fee JA, Woodruff WH. An infrared study of the binding and photodissociation of carbon monoxide in cytochrome ba_3 from *Thermus thermophilus*. J Biol Chem. 1989; 264:2405–2408. [PubMed: 2536707]

34. Yoshikawa S, Choc MG, O'Toole MC, Caughey WS. An infrared study of CO binding to heart cytochrome *c* oxidase and hemoglobin A. J Biol Chem. 1977; 252:5498–5508. [PubMed: 195952]

35. Brzezinski P, Gennis RB. Cytochrome *c* oxidase: exciting progress and remaining mysteries. J Bioenerg Biomembr. 2008; 40:521–531. [PubMed: 18975062]

36. Gibson QH, Greenwood C. Reactions of cytochrome oxidase with oxygen and carbon monoxide. Biochem J. 1963; 86:541–554. [PubMed: 13947736]

37. Hill BC, Greenwood C. The reaction of fully reduced cytochrome *c* oxidase with oxygen studied by flow-flash spectrophotometry at room temperature. Biochem J. 1984; 218:913–921. [PubMed: 6326750]

38. Szundi I, Funatogawa C, Cassano J, McDonald W, Ray J, Hiser C, Ferguson-Miller S, Gennis RB, Einarsdóttir Ó. Spectral identification of intermediates generated during the reaction of dioxygen with the wild-type and EQ(I-286) mutant of *Rhodobacter sphaeroides* cytochrome *c* oxidase. Biochemistry. 2012; 51:9302–9311. [PubMed: 23057757]

39. Szundi I, Van Eps N, Einarsdóttir Ó. pH dependence of the reduction of dioxygen to water by cytochrome *c* oxidase. 2. Branched electron transfer pathways linked by proton transfer. Biochemistry. 2003; 42:5074–5090. [PubMed: 12718551]

40. Szundi I, Funatogawa C, Fee JA, Soulimane T, Einarsdóttir Ó. CO impedes superfast O_2 binding in ba_3 cytochrome oxidase from *Thermus thermophilus*. Proc Natl Acad Sci U S A. 2010; 107:21010–21015. [PubMed: 21097703]

41. Caughey, WS. Methods for Determining Metal Ion Environments in Proteins: Structure and Function of Metallo-proteins. Darnall, DW.; Wilkins, RG., editors. Elsevier/North-Holland; New York: 1980. p. 95-115.

42. Fiamingo FG, Altschuld RA, Moh PP, Alben JO. Dynamic interactions of CO with a3Fe and CuB in cytochrome *c* oxidase in beef heart mitochondria studied by Fourier transform infrared spectroscopy at low temperature. J Biol Chem. 1982; 257:1639–1650. [PubMed: 6276395]

43. Dyer RB, Einarsdóttir Ó, Killough PM, López-Garriga JJ, Woodruff WH. Transient binding of photodissociated CO to CuB+ of eukaryotic cytochrome oxidase at ambient temperature. Direct evidence from time-resolved infrared spectroscopy. J Am Chem Soc. 1989; 111:7657–7659.
44. Dyer RB, López-Garriga JJ, Einarsdóttir Ó, Woodruff WH. The orientation of CO in carbonmonoxy cytochrome oxidase and its transient photoproducts. Direct evidence from time-resolved infrared linear dichroism. J Am Chem Soc. 1989; 111:8962–8963.
45. Dyer RB, Petersen KA, Stoutland PO, Woodruff WH. Ultrafast photoinduced ligand transfer in carbonmonoxy cytochrome *c* oxidase. Observation by picosecond infrared spectroscopy. J Am Chem Soc. 1991; 113:6276–6277.
46. Dyer RB, Peterson KA, Stoutland PO, Woodruff WH. Picosecond infrared study of the photodynamics of carbonmonoxy-cytochrome *c* oxidase. Biochemistry. 1994; 33:500–507. [PubMed: 8286380]
47. Woodruff, WH.; Dyer, RB.; Einarsdóttir, Ó. Spectroscopy, dynamics, and function of cytochrome oxidase. In: Clark, RJH.; Hester, RE., editors. Biological Spectroscopy, Part B. John Wiley and Sons Ltd; Chichester, England: 1993. p. 189-233.
48. Woodruff WH, Einarsdóttir Ó, Dyer RB, Bagley KA, Palmer G, Atherton SJ, Goldbeck RA, Dawes TD, Kliger DS. Nature and functional implications of the cyto- chrome a_3 transients after photodissociation of CO-cytochrome oxidase. Proc Natl Acad Sci U S A. 1991; 88:2588–2592. [PubMed: 1848709]
49. Liu B, Zhang Y, Sage JT, Soltis SM, Doukov T, Chen Y, Stout CD, Fee JA. Structural changes that occur upon photolysis of the Fe(II)$_{a3}$–CO complex in the cytochrome ba_3-oxidase of *Thermus thermophilus*: a combined X-ray crystallographic and infrared spectral study demonstrates CO binding to Cu_B. Biochim Biophys Acta. 2012; 1817:658–665. [PubMed: 22226917]
50. Einarsdóttir Ó, Dyer B, Killough PM, Fee JA, Woodruff WH. Fourier transform infrared and resonance Raman characterization of cytochrome ba_3 from *Thermus thermophilus*. SPIE Proc. 1989; 1055:254–262.
51. Oertling WA, Surerus KK, Einarsdóttir Ó, Fee JA, Dyer RB, Woodruff WH. Spectroscopic characterization of cytochrome ba_3, a terminal oxidase from *Thermus thermophilus*: comparison of the a_3/Cu_B site to that of bovine cytochrome aa_3. Bio- chemistry. 1994; 33:3128–3141.
52. Stoutland PO, Lambry J-C, Martin J-L, Woodruff WH. Femtosecond dynamics of reduced cytochrome oxidase and its CO derivatives. J Phys Chem. 1991; 1991:6406–6408.
53. Koutsoupakis K, Stavrakis S, Pinakoulaki E, Soulimane T, Varotsis C. Observation of the equilibrium Cu_B–CO complex and functional implications of the transient heme a_3 propionates in cytochrome ba_3–CO from *Thermus thermophilus*. Fourier transform infrared (FTIR) and time-resolved step-scan FTIR studies. J Biol Chem. 2002; 277:32860–32866. [PubMed: 12097331]
54. Bailey JA, Tomson FL, Mecklenburg SL, MacDonald GM, Katsonouri A, Puustinen A, Gennis RB, Woodruff WH, Dyer RB. Time-resolved step-scan Fourier transform infrared spectroscopy of the CO adducts of bovine cytochrome *c* oxidase and of cytochrome bo_3 from *Escherichia coli*. Biochemistry. 2002; 41:2675–2683. [PubMed: 11851414]
55. Muramoto K, Ohta K, Shinzawa-Itoh K, Kanda K, Taniguchi M, Nabekura H, Yamashita E, Tsukihara T, Yoshikawa S. Bovine cytochrome *c* oxidase structures en- able O_2 reduction with minimization of reactive oxygens and provide a proton- pumping gate. Proc Natl Acad Sci U S A. 2010; 107:7740–7745. [PubMed: 20385840]
56. Birukou I, Maillett DH, Birukova A, Olson JS. Modulating distal cavities in the alpha and beta subunits of human HbA reveals the primary ligand migration pathway. Biochemistry. 2011; 50:7361–7374. [PubMed: 21793487]
57. Vos MH. Ultrafast dynamics of ligands within heme proteins. Biochim Biophys Acta. 2008; 1777:15–31. [PubMed: 17996720]
58. Lemon DD, Calhoun MW, Gennis RB, Woodruff WH. The gateway to the active site of heme–copper oxidases. Biochemistry. 1993; 32:11953–11956. [PubMed: 8218269]
59. Giuffrè A, Forte E, Antonini G, D'Itri E, Brunori M, Soulimane T, Buse G. Kinetic properties of ba_3 oxidase from *Thermus thermophilus*: effect of temperature. Bio- chemistry. 1999; 38:1057–1065.

60. Einarsdóttir Ó, Funatogawa C, Soulimane T, Szundi I. Kinetic studies of the reactions of O_2 and NO with reduced *Thermus thermophilus* *ba*$_3$ and bovine *aa*$_3$ using photolabile carriers. Biochim Biophys Acta. 2012; 1817:672–679. [PubMed: 22201543]

61. Siletsky SA, Belevich I, Jasaitis A, Konstantinov AA, Wikström M, Soulimane T, Verkhovsky MI. Time-resolved single-turnover of *ba*$_3$ oxidase from *Thermus thermophilus*. Biochim Biophys Acta. 2007; 1767:1383–1392. [PubMed: 17964277]

62. Greenwood C, Gibson QH. The reaction of reduced cytochrome *c* oxidase with oxygen. J Biol Chem. 1967; 242:1782–1787. [PubMed: 4290651]

63. Blackmore RS, Greenwood C, Gibson QH. Studies of the primary oxygen intermediate in the reaction of fully reduced cytochrome oxidase. J Biol Chem. 1991; 266:19245–19249. [PubMed: 1655779]

64. Bailey JA, James CA, Woodruff WH. Flow-flash kinetics of O_2 binding to cytochrome *c* oxidase at elevated [O_2]: observations using high-pressure stopped- flow for gaseous reactants. Biochem Biophys Res Commun. 1996; 220:1055–1060. [PubMed: 8607790]

65. Koutsoupakis K, Stavrakis S, Soulimane T, Varotsis C. Oxygen-linked equilibrium Cu_B–CO species in cytochrome *ba*$_3$ oxidase from T*hermus thermophilus*. Implications for an oxygen channel ar the Cu_B site. J Biol Chem. 2003; 278:14893–14896. [PubMed: 12594218]

66. Hunsicker-Wang LM, Pacoma RL, Chen Y, Fee JA, Stout CD. A novel cryoprotection scheme for enhancing the diffraction of crystals of recombinant cytochrome *ba*$_3$ oxidase from *Thermus thermophilus*. Acta Crystallogr. 2005; D61:340–343.

67. Muramoto K, Hirata K, Shinzawa-Itoh K, Yoko-o S, Yamashita E, Aoyama H, Tsukihara T, Yoshikawa S. A histidine residue acting as a controlling site for dioxygen reduction and proton pumping by cytochrome *c* oxidase. Proc Natl Acad Sci U S A. 2007; 104:7881–7886. [PubMed: 17470809]

68. Liu B, Chen Y, Doukov T, Soltis SM, Stout CD, Fee JA. Combined microspectrophotometric and crystallographic examination of chemically reduced and X-ray radiation-reduced forms of cytochrome *ba*$_3$ oxidase from *Thermus thermophilus*: structure of the reduced form of the enzyme. Biochemistry. 2009; 48:820–826. [PubMed: 19140675]

69. Goldbeck RA, Einarsdóttir Ó, Dawes TD, O'Connor DB, Surerus KK, Fee JA, Kliger DS. Magnetic circular dichroism study of cytochrome *ba*$_3$ from *Thermus thermophilus*: spectral contributions from cytochromes *b* and *a*$_3$ and nanosecond spectroscopy of CO photodissociation intermediates. Biochemistry. 1992; 31:9376–9387. [PubMed: 1327113]

70. Blomberg LM, Blomberg MR, Siegbahn PE. A theoretical study on nitric oxide reductase activity in a *ba*$_3$-type heme–copper oxidase. Biochim Biophys Acta. 2006; 1757:31–46. [PubMed: 16375849]

71. Hayashi T, Lin IJ, Chen Y, Fee JA, Moënne-Loccoz P. Fourier transform infrared characterization of a Cu_B–nitrosyl complex in cytochrome *ba*$_3$ from *Thermus thermophilus*: relevance to NO reductase activity in heme–copper terminal oxidase. J Am Chem Soc. 2007; 129:14952–14958. [PubMed: 17997553]

72. Surerus KK, Oertling WA, Fan C, Gurbiel RJ, Einarsdottir Ó, Antholine WE, Dyer RB, Hoffman BM, Woodruff WH, Fee JA. Reaction of cyanide with cytochrome *ba*$_3$ from *Thermus thermophilus*: spectroscopic characterization of the Fe(II)a_3–CN·Cu(II)$_B$–CN complex suggests four ^{14}N atoms are coordinated to Cu_B. Proc Natl Acad Sci U S A. 1992; 89:3195–3199. [PubMed: 1314380]

73. Brudvig GW, Stevens TH, Chan SI. Reactions of nitric oxide with cytochrome *c* oxidase. Biochemistry. 1980; 19:5275–5285. [PubMed: 6255988]

74. Young LJ, Caughey WS. Oxygenation of carbon monoxide by bovine heart cytochrome *c* oxidase. Biochemistry. 1986; 25:152–161. [PubMed: 3006748]

75. Pilet E, Nitschke W, Rappaport F, Soulimane T, Lambry JC, Liebl U, Vos MH. NO binding and dynamics in reduced heme–copper oxidases *aa*$_3$ from *Paracoccus denitrificans* and *ba*$_3$ from *Thermus thermophilus*. Biochemistry. 2004; 43:14118–14127. [PubMed: 15518562]

76. Hayashi T, Lin MT, Ganesan K, Chen Y, Fee JA, Gennis RB, Moenne-Loccoz P. Accommodation of two diatomic molecules in cytochrome *bo*: insights into NO reductase activity in terminal oxidases. Biochemistry. 2009; 48:883–890. [PubMed: 19187032]

77. Sharrock M, Yonetani T. Low-temperature flash photolysis studies of cytochrome oxidase and its environment. Biochim Biophys Acta. 1977; 462:718–730. [PubMed: 202310]

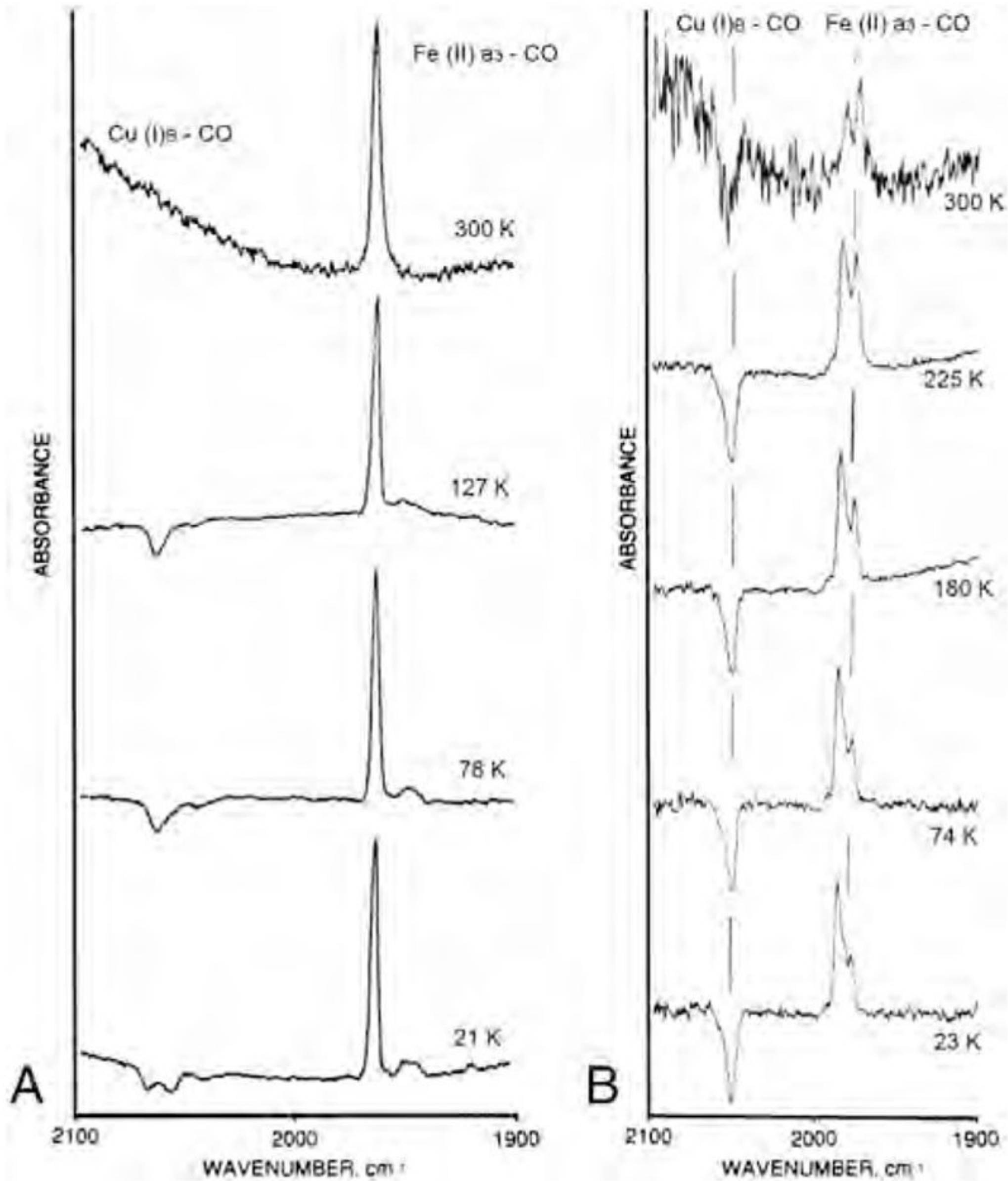

Fig. 1.

FTIR difference spectra (dark minus light) of carbonmonoxy fully reduced bovine cytochrome aa_3 (left) and *Thermus thermophilus* cytochrome ba_3 (right) at various temperatures. The 300 K light spectrum of the ba_3 enzyme was recorded under continuous photolysis. Conditions are those described in [32] and [33].

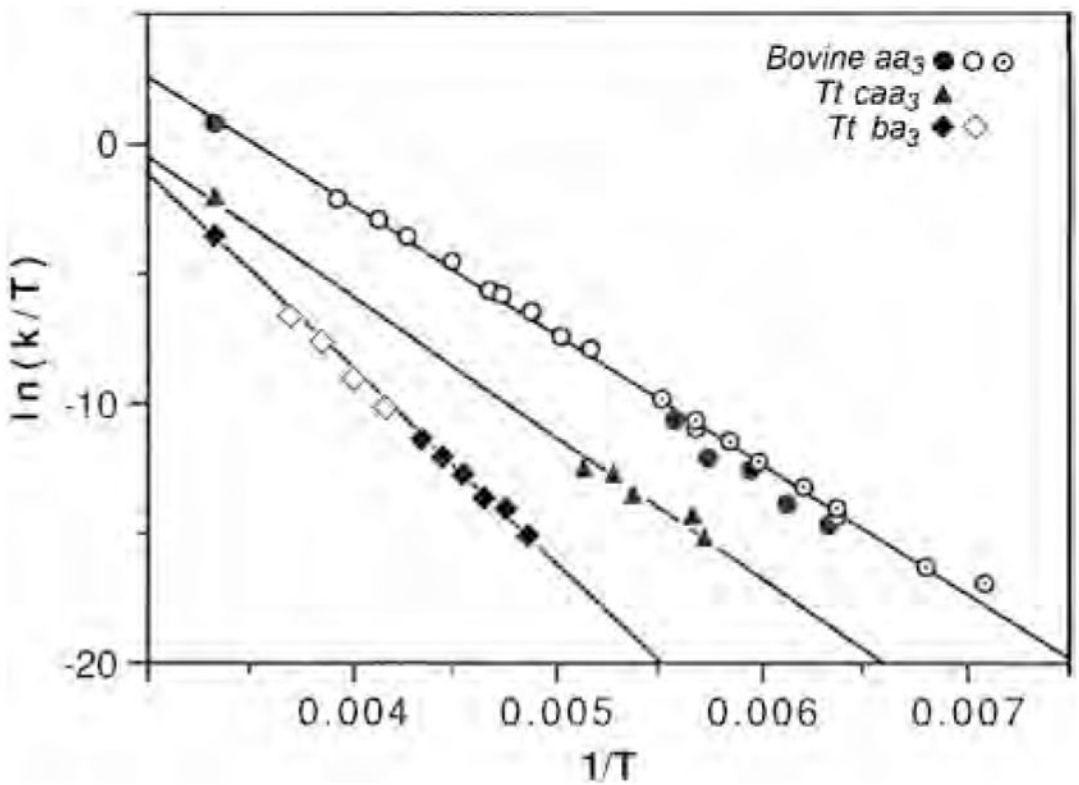

Fig. 2.
The Eyring plot for *T. thermophilus* cytochrome ba_3–CO, *T. thermophilus* caa_3–CO and bovine aa_3–CO recombination, measured from the Fe–CO infrared peaks (low temperature) and by kinetic UV–vis spectrophotometry at room temperature. Data are from current work and [32,33]. For the bovine enzyme, open circles are from Sharrock and Yonetani [77] and the circles with concentric dots are from Fiamingo et al. [42].

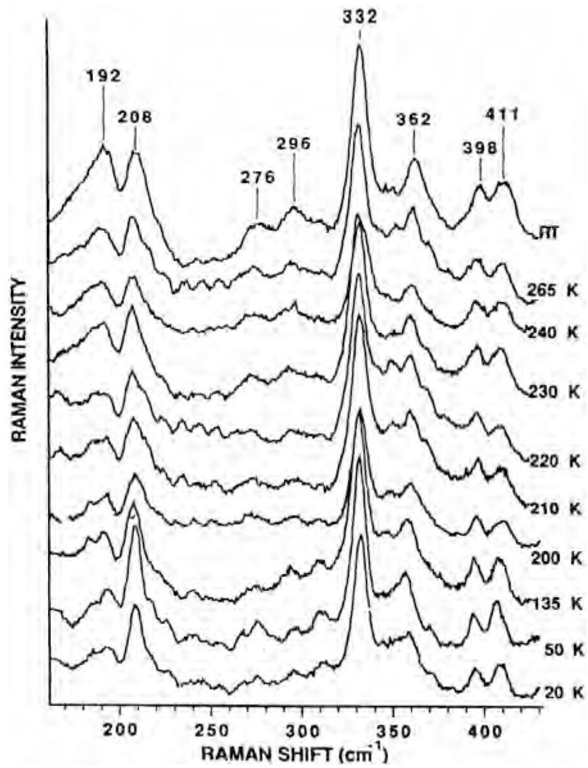

Fig. 3.

Resonance Raman spectra showing the Fe–N(Im) stretching peaks of *T. thermophilus* cytochrome ba_3 as a function of temperature.

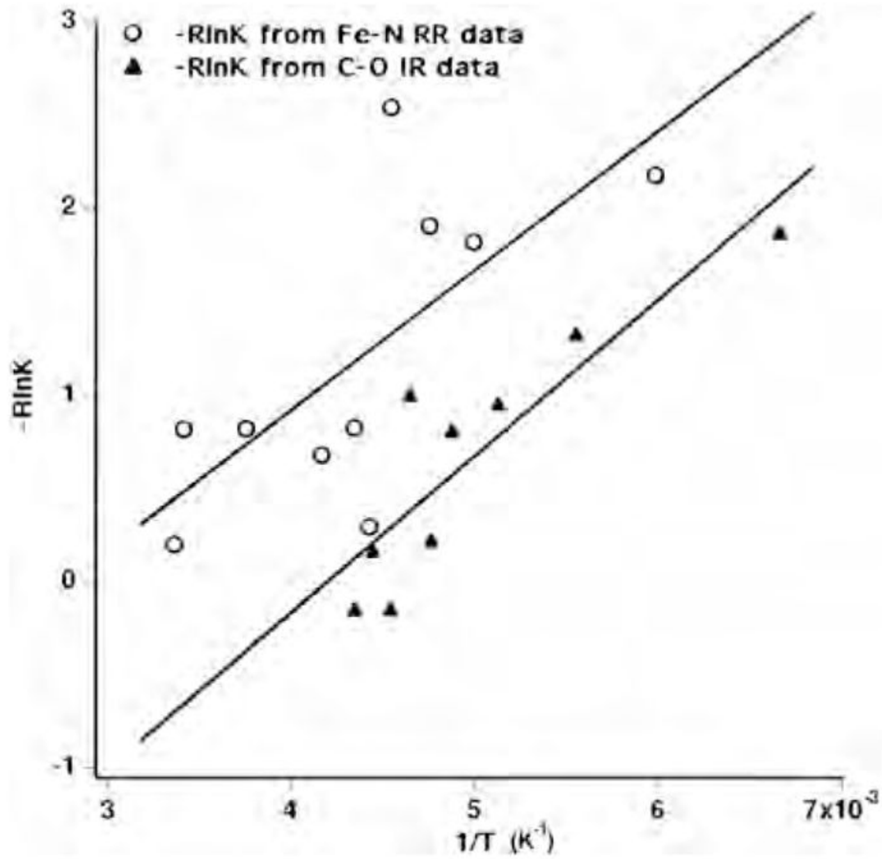

Fig. 4.

Conformer thermodynamics. The temperature dependent intensities of the 192 and 208 cm^{-1} Fe-N(Im) bands in the resonance Raman spectra of *Tt* ba_3 and those of the two major Fe-CO stretching peaks at 1973 and 1984 cm^{-1}.

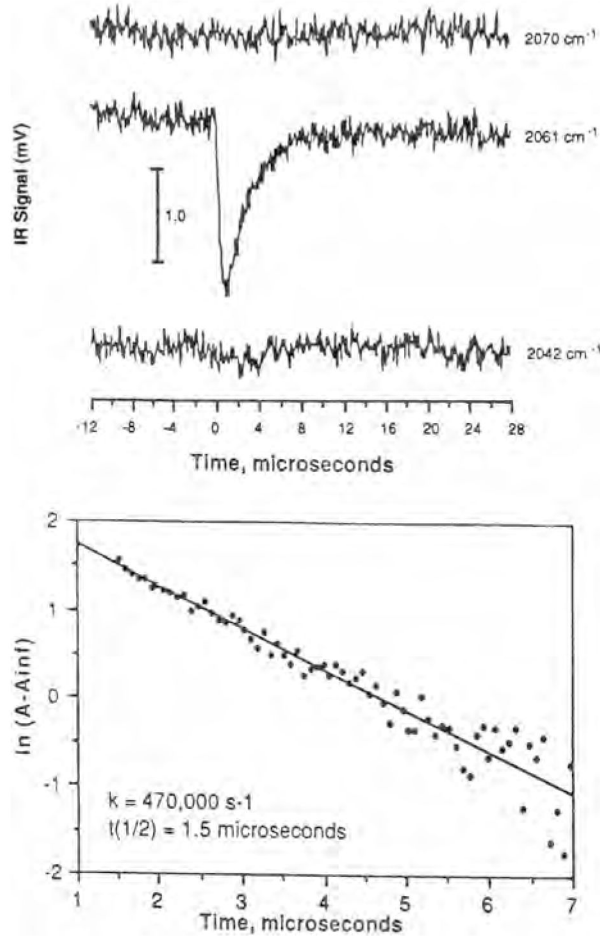

Fig. 5.
(Top) The room temperature transients of bovine heart cytochrome aa_3–CO following photolysis of CO from the heme. (Bottom) A single exponential fit to the Cu_B^+-CO transient decay (see ref. [43]) for details.

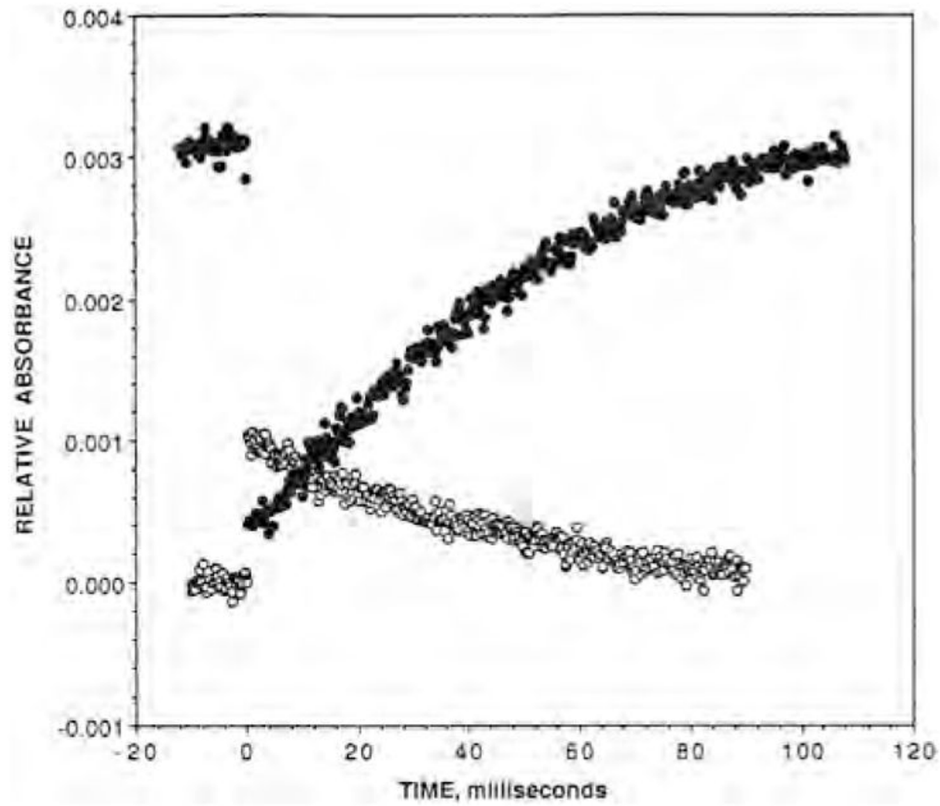

Fig. 6.

The post-photodissociation TRIR transient absorbance trace recorded at the maximum of the Fe_{a3}–CO absorbance peak at 1974 cm^{-1} (filled circles) and the Cu_B^+-CO absorbance peak at 2053 cm^{-1} (open circles).

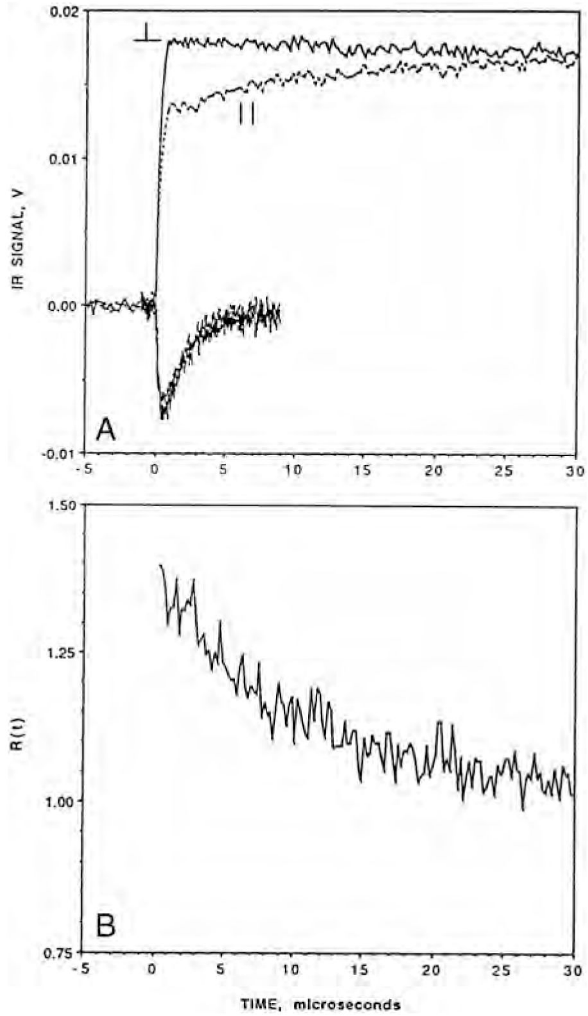

Fig. 7.

(A) The TRIR linear dichroism signals of CO-bound bovine heart cytochrome oxidase between −5 and 30 μs with respect to the time of the photodissociation pulse. The upper traces are for the Fe–CO complex and the lower traces for the Cu_B–CO photoproduct. The polarization of the infrared probe beam relative to the photo-dissociation pulse is indicated. The solid traces represent perpendicular polarization and the dashed traces represent the parallel polarization. (B) The time-dependence of the polarization ratio, R(t) $=(\Delta A_{perpendicular} / \Delta A_{parallel})$ (see ref. [44] for further details).

Modified from [44].

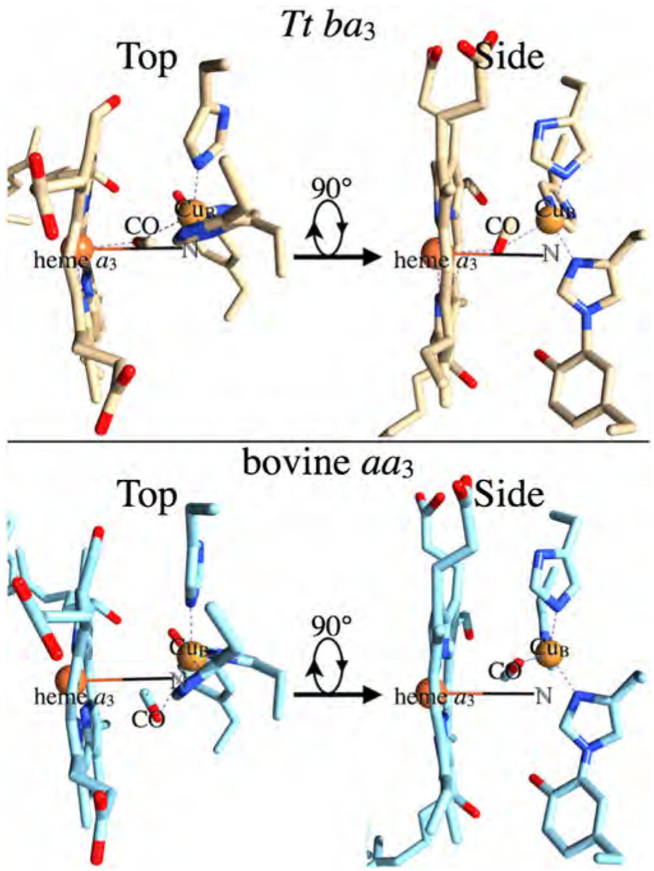

Fig. 8.

Top panel: The *Tt ba*$_3$ Cu$_B$–CO transient photoproduct (PDB 3QJR, *49*). Lower panel: The bovine Cu$_B$–CO transient photoproduct (PDB 3AG2, *55*). In both panels, the left figure (Top) is viewed from the positive side of membrane, while the right figure (Side) is viewed from the ligand entrance channel. The "Side" view is generated from the "Top" by a left-handed 90° rotation about the horizontal axis.

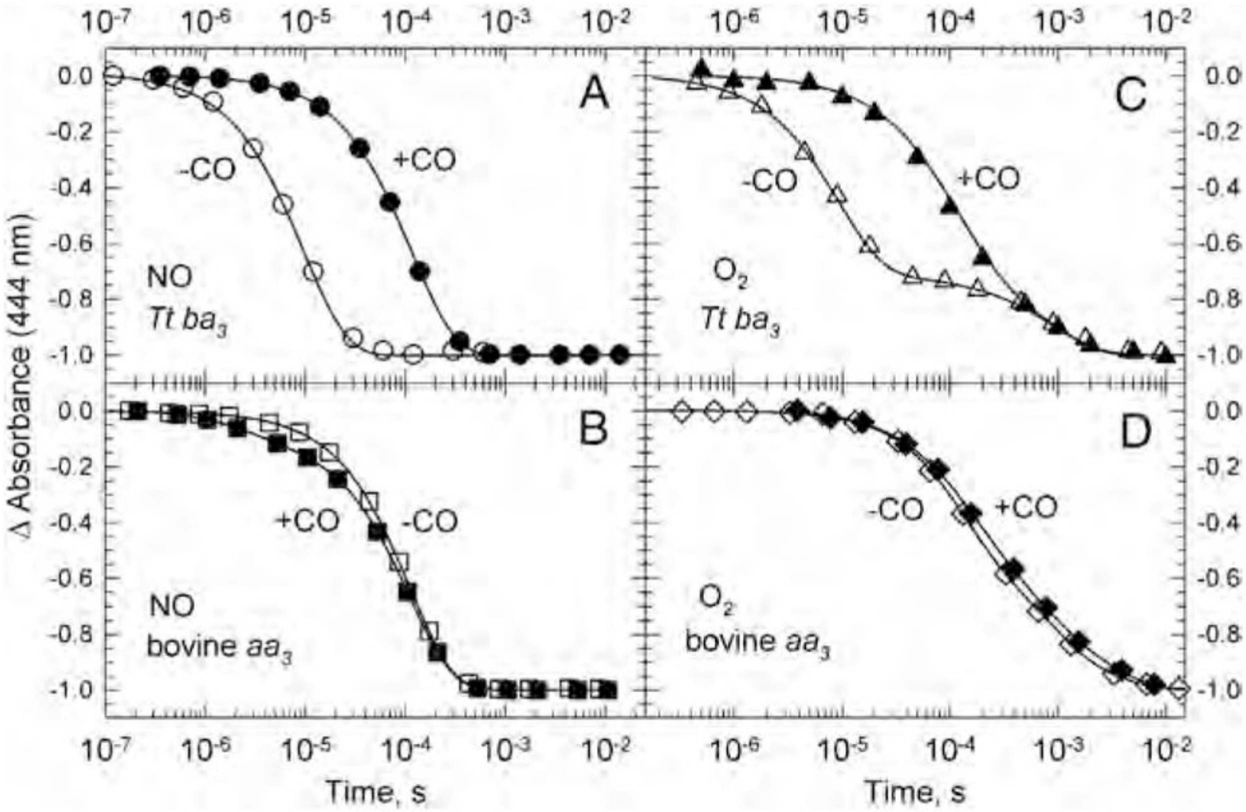

Fig. 9.
Comparison of the transient absorbance changes at 444 nm during the reaction of the fully reduced *ba*$_3$ (panels A and C) and bovine *aa*$_3$ (panels B and D) with photoproduced NO (A and B) and photoproduced O_2 (C and D) in the presence of CO (filled symbols) and absence of CO (open symbols). The kinetics traces are from time-resolved optical absorption data recorded at multiple wavelengths and are normalized to the total absorbance change. The solid lines represent the absorbance traces at 444 nm calculated on the basis of a single exponential fit. The conditions are those reported in [40,60].

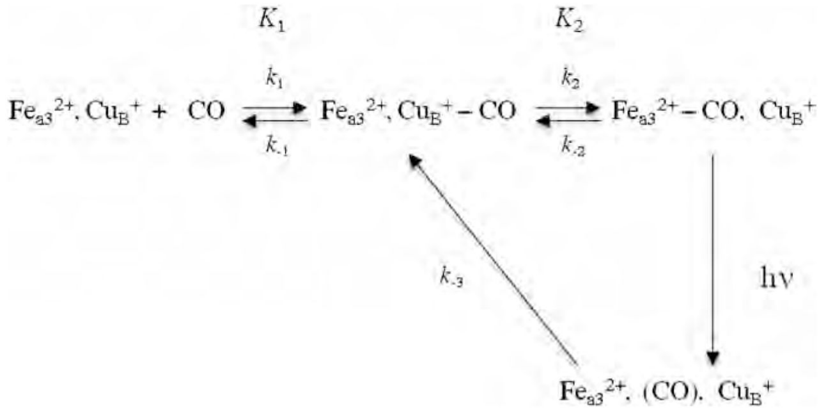

Scheme 1.
Proposed mechanism for CO photodissociation and rebinding in heme-copper oxidases.

NIH-PA Author Manuscript

NIH-PA Author Manuscript

Table 1

Activation parameters for *Tt* ba_3, *Tt* caa_3 and bovine aa_3.

	ΔH‡ (kcal/mol)	**ΔS‡ (cal/mol-K)**
T. thermophilus ba_3	14.9	−5
T. thermophilus caa_3	10.8	−16
Bovine aa_3	10.0	−12